Mathematical Biosciences and Engineering

http://www.aimspress.com/journal/MBE

Mathematical Biosciences and Engineering, 5(x): xxx–xxx
DOI:
Received: xx 2019
Accepted: xx 2019
Published: xx 2019

Type of article

A Data-Driven Model of Glioblastoma Multiforme Growth with Explicit Birth and Death Rates*

Lifeng Han[1], Steffen Eikenberry[1], Changhan He[1], Lauren Johnson[1], Mark Preul[2], Eric Kostelich [1], and Yang Kuang[1,*]

[1] School of Mathematical and Statistical Sciences, Arizona State University, Tempe, AZ 85287, USA

[2] Department of Neurosurgery Research, Barrow Neurological Institute, St. Josephs Hospital and Medical Center, Phoenix, AZ 85013, USA

* **Correspondence:** kuang@asu.edu; Tel: +1-111-111-1111; Fax: +1-111-111-1111.

Abstract: Glioblastoma multiforme (GBM) is an aggressive brain cancer with grim prognosis. Its morphology is characterized by layered structure, i.e., an inner necrotic core and an outer rim of proliferating cells. This structure can be observed in magnetic resonance images images. A mathematical model of GBM growth with explicit birth and death rate is proposed. This model demonstrates a traveling wave. We develop a method to compute some characteristics of the approximate wave profile, which can be matched with image data. Various forms of growth and death terms and their parameter identifiability are studied. We use image data of GBM patients to get personalized parameterization of the model, of which the biological and clinical implications are discussed.

Keywords: Glioblastoma multiforme modeling; parameter estimation; traveling wave; necrosis; proliferation

1. Introduction

Glioblastoma multiforme (GBM) is a type of the most aggressive brain cancer. Patients with GBM have a mean survival length less than 15 months from the time of diagnosis [15]. Its fast progression is characterized by highly proliferating and invasive cancer cells. Its tumor morphology manifests a layered structure: there is a necrotic core at the center, a band of proliferating cells at the outer rim and a transition layer of quiescent cancer cells in between. The tumor can be visualized by magnetic resonance (MR) imaging, which is commonly used to inform clinical decisions. One of the hallmarks of GBM is its heterogeneity between individual patients, imposing a challenge to its treatment.

Mathematical modeling can offer a way to tackle this challenge. Mathematical modeling has pro-

vided a lot of insight to our understanding of cancer and its treatment [10]. Mathematical models on GBM are abundant (see [12] for a review). A popular type of those models employs reaction-diffusion equations. In many cases [6, 5, 20], those systems exhibit a traveling wave solution of which the speed is of great interests since it is related to how fast cancer progress.

However, models which confront the heterogeneity of GBM directly by utilizing spatio-temporal patient-specific data are rare. Swanson and her collaborators [22, 14, 7] is one of the few teams which focus on this endeavor. They used the well-known Fisher's equation [4] (called PI model in [7]) and parameterized it using MR images. The estimated proliferation and diffusion parameters and a model-derived metric called days gained are deemed to be instrumental to clinical treatments. But their treating the cancer cells as a single species is an oversimplification and by doing so the structured morphology of GBM has to be ignored. Although there are modeling works taking into account of multi-species nature of cancer cells [3, 21], they are oftentimes too complicated to be practically useful given scarcity of image data of an individual patient. To fill this gap, we propose a model which includes two species of cancer cells, i.e., proliferating and quiescent, and is capable of exploiting the structural information offered by one or two MR scans.

Gliomas can only be imaged indirectly on MRI, and are typically characterized, on T1-weighted sequences, by a large, often necrotic core region surrounded by a bright enhancing rim that correlates with high blood vessel density and (presumably) rapid cell proliferation. Finally, this core and rim is usually surrounded by a large expanse of edema that is visible on T2-weighted MRI, and may represent diffusely invasive, highly motile cells. Thus, we have three basic signals from imaging: necrotic radius, enhancing radius, and T2 (or maximum) radius. We hypothesized that a relatively simple mathematical model framework can capture all three signals, and yield insight into the relative contributions of cellular proliferation, motility, and necrosis to each major feature.

The paper is organized as following. We first describe our model and its assumptions. Then we demonstrate that the model has a traveling wave solution and work out its approximate wave profile. We devise a simple procedure to estimate the parameters by fitting the approximate wave profile to image data, for which identifiability is checked. This procedure is then applied to several patient-specific data.

2. Model and method

2.1. Model description

To model the growth of GBM, we propose a system of reaction-diffusion equations

$$\frac{\partial p}{\partial t} = \nabla \cdot \left[\frac{Dp}{p+q} \nabla (p+q) \right] + \tilde{g}(w)p - \tilde{\delta}(w)p \tag{2.1a}$$

$$\frac{\partial q}{\partial t} = \nabla \cdot \left[\frac{Dq}{p+q} \nabla (p+q) \right] + \tilde{\delta}(w)p, \tag{2.1b}$$

where two species are considered: proliferating cells and quiescent cells whose density at time t and location x is represented by $p(x,t)$ and $q(x,t)$ respectively. We assume the flux of total population due to migration is $-D\nabla(p+q)$ where D is a constant diffusion coefficient. It is further assumed that the proportion of the total flux contributed by each species equals their proportion of the total population. This diffusion term is believed to be a realistic account of cancer cell movements [18].

Per capita birth rate is $\tilde{g}(w)$ and the proliferating cells become quiescent with per capita rate $\tilde{\delta}(w)$. Both of them is a function of w. We define $w = 1 - p - q$, interpreted as availability of space or some generic nutrient (we call it growth factor henceforth). By doing so, we have scaled the maximum cell density to be 1. In our model, necrosis is not explicitly included but can be thought of being lumped into q. This choice is supported by the fact that MR only visualizes proliferating cells and does not distinguish between quiescence and necrosis, and the decision to keep the model simple enough so that it makes use of available information without over-complicating the problem. Note that quiescent cells can not become proliferating again but only turns into necrosis. Therefore $\tilde{\delta}(w)$ can be thought of as death rate.

In order to achieve biological meaning, we impose the following constraints on $g(w)$ and $\delta(w)$:

$$\tilde{g}'(w) \geq 0, \tilde{\delta}'(w) \leq 0, \tilde{g}(1) \geq \tilde{\delta}(1) = 0, \tilde{\delta}(0) > \tilde{g}(0) = 0. \tag{2.2}$$

That is, birth/death should increase/decrease with availability of the growth factor, and there is more birth than death at maximum growth factor while there is only death and no growth in absence of growth factor. It is also assumed that death rate is negligible at maximum growth factor. With those assumptions, it can be shown that the solution of (2.1) stay nonnegtive and is bounded by $p + q \leq 1$ for all t with suitable initial condition.

We can estimate three parameters based on the three pieces of information we can derive from MR images. Therefore we want a few more restrictions on $\tilde{g}(w)$ and $\tilde{\delta}(w)$ for the ease of parameter estimation and ensure their identifiability. Since we can only introduce two more parameters in addition to diffusion coefficient D, we introduce ρ and k into $\tilde{g}(w)$ and $\tilde{\delta}(w)$ respectively and indicate their dependence on the parameters as $\tilde{g}(w;\rho)$ and $\tilde{\delta}(w;k)$. It is desirable to make the proliferating rate at maximum growth factor and death rate at zero growth factor be ρ and δ, i.e., $\tilde{g}(1,\rho) = \rho$, $\tilde{\delta}(0;k) = k$. For reasons that will become clear later, we pick the functional form which can be written as $\tilde{g}(w;\rho) = \rho g(w)$ and $\tilde{\delta}(w;k) = k\delta(w)$. Although we have stated several additional assumptions, it should be noted that they impose little impact on the generality and flexibility of our model. The benefit of including them will become clear in the section of parameter estimation.

2.2. Approximate wave profile

We consider one spatial dimension for simplicity. It is justified by the fact that the tumor is mostly spherical and at the time of diagnosis its radius is large enough so that radial effect is negligible. Together with the aforementioned assumptions, the equations now write as

$$\frac{\partial p}{\partial t} = \frac{\partial}{\partial x}\left[\frac{Dp}{p+q}\frac{\partial}{\partial x}(p+q)\right] + \rho g(w)p - k\delta(w)p \tag{2.3a}$$

$$\frac{\partial q}{\partial t} = \frac{\partial}{\partial x}\left[\frac{Dq}{p+q}\frac{\partial}{\partial x}(p+q)\right] + k\delta(w)p, \tag{2.3b}$$

We nondimensionlize the system using the characteristic length $\sqrt{D/k}$ and the characteristic time $1/k$ so that $x = \sqrt{D/k}\hat{x}$ and $t = \hat{t}/k$, which leads to

$$\frac{\partial p}{\partial \hat{t}} = \frac{\partial}{\partial \hat{x}}\left[\frac{p}{p+q}\frac{\partial}{\partial \hat{x}}(p+q)\right] + \hat{\rho} g(w)p - \delta(w)p \tag{2.4a}$$

$$\frac{\partial q}{\partial \hat{t}} = \frac{\partial}{\partial \hat{x}}\Big[\frac{q}{p+q}\frac{\partial}{\partial \hat{x}}(p+q)\Big] + \delta(w)p, \tag{2.4b}$$

where $\hat{\rho} = \rho/k$. We are seeking a traveling wave solution, i.e., $p(\xi) = p(\hat{x} - c\hat{t}), q(\xi) = q(\hat{x} - c\hat{t})$ where c is wave speed and there is a slight abuse of notation. Substituting these into (2.4) gives

$$(\frac{p}{p+q}(p+q)')' + cp' + \hat{\rho}g(w)p - \delta(w)p = 0 \tag{2.5a}$$

$$(\frac{q}{p+q}(p+q)')' + cq' + \delta(w)p = 0, \tag{2.5b}$$

where the prime indicates the derivative with respect to ξ. Linearizing at the wave head, i.e., substitute an ansztz $p = Ae^{-r\xi}$ and $q = Be^{-r\xi}$ into (2.5) gives $(r^2 - cr + \rho)A = 0$. The nontrivial A entails the minimum speed of the wave $c_{\min} = 2\sqrt{\hat{\rho}}$. It is numerically verified that the minimum speed is exactly the asymptotic speed, i.e., $c = c_{\min}$.

To obtain a approximate wave profile, we adopt a method first used by [1]. We rescale the wave coordinate $z = -\xi/c$, which leads to

$$\frac{1}{c^2}(\frac{p}{p+q}(p+q)')' - p' + \hat{\rho}g(w)p - \delta(w)p = 0 \tag{2.6a}$$

$$\frac{1}{c^2}(\frac{q}{p+q}(p+q)')' - q' + \delta(w)p = 0, \tag{2.6b}$$

where the prime indicates the derivative with respect to z. Assuming that $1/c^2$ is small, we neglect the first terms of (2.6a),(2.6b). Writing the system in terms of p and w, we get the reduced system as below

$$\frac{dp}{dz} = p(\hat{\rho}g(w) - \delta(w)) \tag{2.7a}$$

$$\frac{dw}{dz} = -\hat{\rho}pg(w), \tag{2.7b}$$

which is amenable to phase plane analysis. The approximate wave solution corresponds to a trajectory that leaves $(0, 1)$ and ends at $(0, w^*)$ with $w^* \in [0, 1)$ (see Figure 1). Its existence based on assumptions (2.2) is shown in the appendix. With a specific choice of $g(w)$ and $\delta(w)$, the trajectory can be found by taking(2.7a) over (2.7b), which gives

$$\frac{dp}{dw} = \frac{\delta(w)}{\hat{\rho}g(w)} - 1.$$

Upon integration we get p as a function of w, i.e., $p = p(w)$, which we will make use of in the next section.

2.3. Parameter estimation

We first discuss the three pieces of information which we can get from MR images and fit our model to. There are two types of MR: T1 highlights high density of proliferating cells while T2 has a lower detection threshold. We denote the their detection thresholds as $100 \times a_1\%$ and $100 \times a_2\%$

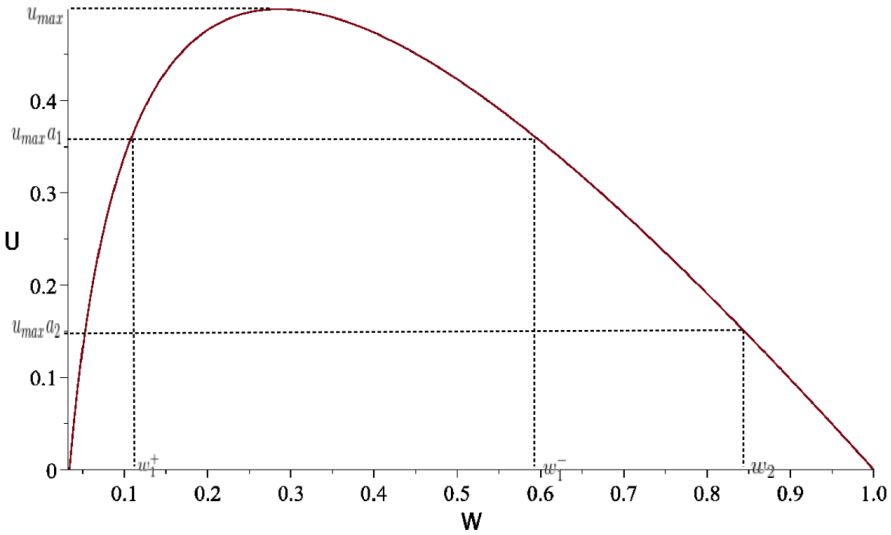

Figure 1. A typical trajectory corresponds to a approximate traveling wave

of $p_{\max} = \max_z\{p(z)\}$ (the actual maximum density of proliferating cells given by the traveling wave solution) with $a_1 > a_2$. To fit our 1-D model, we convert necrotic core volume, T1 volume and T2 volume into equivalent spheres with their radius denoted by R_0, R_1 and R_2 (to do: figure needed). Therefore, the width of proliferating rim denoted as L_1 and L_2 for T1 and T2 images can be calculated, i.e., $L_1 = R_1 - R_0$ and $L_2 = R_2 - R_1$. Typically, there are two MR scans before surgery: one is at diagnosis and the other is right before surgery with a usual time interval of a few weeks [22]. The image-derived wave velocity V is the change in tumor radius divided by the length of this time interval.

From our approximate wave profile, we can compute the corresponding quantities to match with images (Figure 2). The rim width (in dimensional form) is computed as below

$$\ell_1 = \frac{\sqrt{D\rho}}{k}\int_{w_1^-}^{w_1^+}\frac{dz}{dw}dw \tag{2.8a}$$

$$\ell_2 = \frac{\sqrt{D\rho}}{k}\int_{w_1^+}^{w_2}\frac{dz}{dw}dw, \tag{2.8b}$$

where $w_1^\pm$ and w_2 satisfy $p(w_1^\pm) = a_1 p_{\max}, p(w_2) = a_2 p_{\max}$ (see also Figure 1). Additionally, model-derived wave speed $c = 2\sqrt{\rho D}$ can be matched with image-derived speed V. Thus we have three nonlinear equations

$$\{\ell_1 = L_1, \ell_2 = L_2, c = V\}, \tag{2.9}$$

from which we hope to find parameters D, ρ and k. Thanks to the assumptions we made before, we can simply take the ratio of (2.8a) and (2.8b), which gives

$$f(\frac{\rho}{k}) \equiv \frac{\int_{w_1^-}^{w_1^+}\frac{dz}{dw}dw}{\int_{w_1^-}^{w_1^+}\frac{dz}{dw}dw} = \frac{L_1}{L_2}, \tag{2.10}$$

where we note that the integrals are a function of ρ/k. (2.10) can be solved for ρ/k analytically in special cases or numerically in general. We note that the monotonicity of $f(\cdot)$ is important for identifiability of parameters. Once we find ρ/k, it can be back substitute to find all parameters.

It is often observed in MR images that the tumor morphology is not perfectly invariant over the course of tumor growth, i.e., the wave profile changes over time. We suspect that the proliferating and diffusion parameters (ρ and D) can change because of mutation while there is little change in k. In this sense, the procedure above can be simply extended. For example, if MR images taken at two different time gives different rim width $\{L_1, L_2\}, \{L_1', L_2'\}$, then we can estimate ρ, D, ρ', D', k by solving the following system of 5 equations

$$\{\ell_1 = L_1, \ell_2 = L_2, \ell_1' = L_1', \ell_2' = L_2', V = \frac{2}{1/c + 1/c'}\},$$

where we have taken the image-derived wave speed be a harmonic mean of model-derived wave speed at the two different times. It is motivated by our belief that the mutation tends be correlated with tumor size other than time.

The above method requires two MR scans taken at two consecutive times before surgery in order to obtain image-derived wave speed. If the second image is not available, another approximation can be made to rescue this situation. Generally, tumor age can be estimated by the tumor radius divided by the wave speed. However, age estimation differs in terms of which radius (say R_1 or R_2) to use. This discrepancy can be explained by the common observation that tumor grows exponentially at the initial stage and then linearly later on [10]. This initial exponential growth stage needs to be taken into account as a correction to the aforementioned tumor age estimation. The initial exponential growth stage potentially affects the age estimation using R_2 more than the one using R_3. Assuming that from $t = 0$ to $t = t^*$, the T1 volume of the tumor expands exponentially and then follows linear growth with speed $2\sqrt{\rho D}$, and that exponential growth stage of T2 volume is negligible, we have

$$\frac{R_1 - r_0(e^{\rho t^*})^{1/3}}{2\sqrt{\rho D}} + t^* = \frac{R_2}{2\sqrt{\rho D}},$$

where r_0 is the initial tumor radius and t^* is the length of the exponential growth stage. Replacing the last equation in (2.9) with the equation above, we have again three equations for which we can solve for the three unknown parameters.

3. Results

We first investigate the monotonicity of $f(\cdot)$ for some specific choice of $g(w)$ and $\delta(w)$ because it is crucial for parameter identifiability. Given our restrictions on $g(w)$ and $\delta(w)$, the cumulative density function (cdf) of Beta distribution family suits our purposes ($\delta(w) = 1 - cdf(w)$). By tweeting the scale and shape of beta distribution we can get linear, sigmoid and concave up/down curves (see left pane of Figure 3). It turns out that our framework is very robust to those choices, i.e., monotonicity of $f(\cdot)$ is well preserved (right pane of Figure 3). As we can see, the sigmoid shaped $g(w)$ and $\delta(w)$ give larger range of $f(\cdot)$ and thus more flexibility in parameter estimation. Moreover, sigmoid curves are believed to be biological relevant (most enzymatic reaction rates have the same shape with respect to reactant concentration). Therefore, we focus on this choice and move on to find patient specific parameters using their MR images.

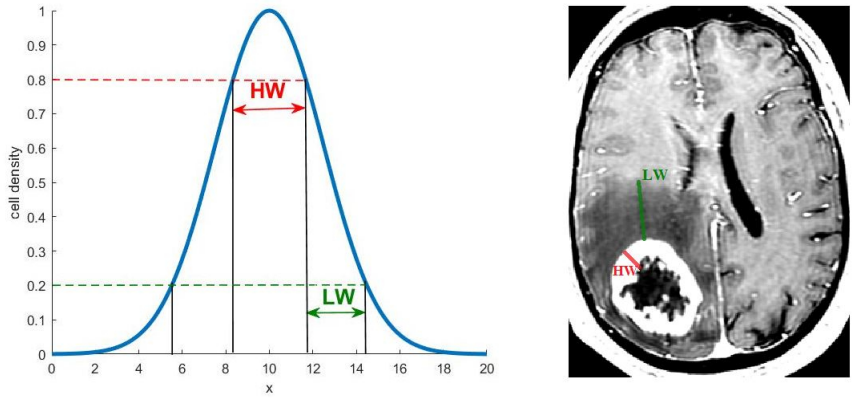

Figure 2. Match model-derived quantities to image-derived quantities (to do: need redo this figure)

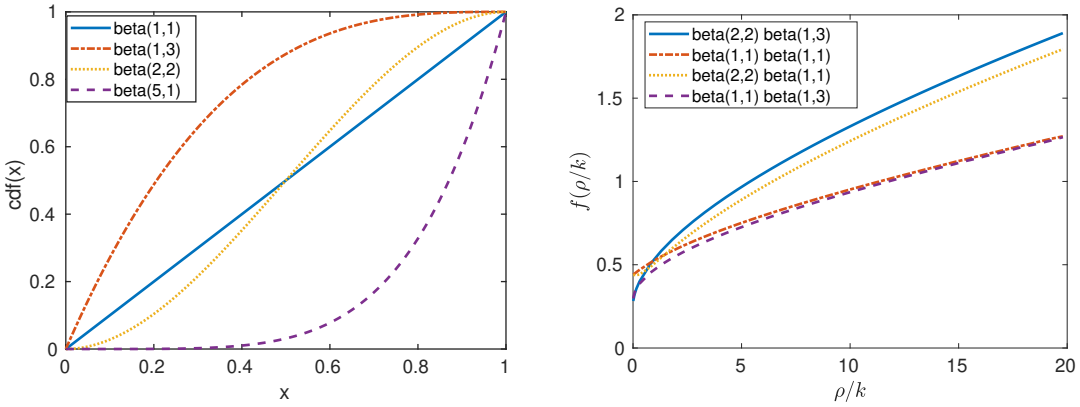

Figure 3. left: cdf of some beta distribution. right: monotonicity of $f(\cdot)$ given different choices of $g(w)$ and $\delta(w)$ as indicated in the legend

We parameterize our model with patient's data in which there is only one MR scan before surgery. In Table 1 we summarize the image-derived tumor radii and the corresponding parameters estimated by the method introduced in the previous section. We observe substantial variation of the parameters among individual patients.

We compare our approximate quantities to those obtained from the numerical solution of the model. As shown in Figure 4, the approximated results match with numerical results well except for some discrepancy for L_2 when $\hat{\rho}$ is small. It is not a surprise since the approximation is based on assumption of large $c = 2\sqrt{\hat{\rho}}$. Moreover, numerical approximation of L_2 is prone to errors due to the fixed grid size and large rate of change around the threshold of L_2. Overall, we are convinced that our approximation is accurate for the parameter range arisen from the image data.

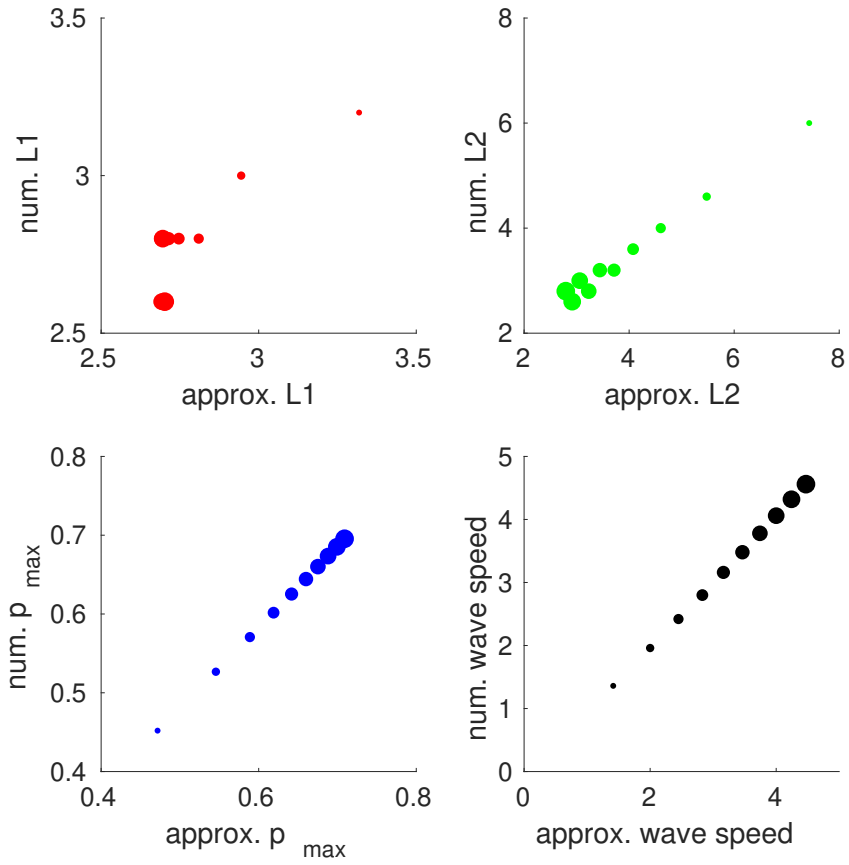

Figure 4. scatter plots of approximate wave profile characteristics (on horizontal axis) verses the ones obtained by numerical simulation (on vertical axis) for a range of $\hat{\rho}$ from 0.5 to 5 by incremental 0.5. The size the the dot corresponds to the value of $\hat{\rho}$.

Table 1. Radii of equivalent tumor sphere derived from T1 and T2 images and their corresponding estimated parameters.

Patient no.	R_0, mm	R_1, mm	R_2, mm	D, mm^{2}s^{-1}	ρ, s^{-1}	k, s^{-1}
1	14.87	15.24	15.83	0.2873	0.0529	0.0152
2	20.73	22.87	20.35	0.9009	0.0462	0.0623
3	27.77	26.96	19.83	0.108	0.0568	0.0107
4	20.48	37.03	23.8	0.6747	0.0445	0.1342
5	26.34	8.17	38.05	0.7374	0.0476	0.0426
6	38.24	14.2	13.31	0.1057	0.0635	0.0041
7	10.91	8.29	34.33	1.2655	0.046	0.0645

4. Discussion

The diffusion term in (2.3) falls into a general category called cross diffusion [11], a phenomenon in which the gradient in the concentration of one species can cause a flux of another species. This type of cross diffusion considered here was studied in a more general and theoretical context [17]. In [18], the authors justified the adoption of this proportion-based cross diffusion in a tumor growth model by recognizing that tumor cell migration is "contact inhibited", i.e., the presence of one type of cell prevents the movements of the other. In other words, the movements of one type of cell drags along other type of cells with it. It is believed that this type of diffusion is more realistic than simple linear diffusion (Fickian) in a sense that it prevents unrealistic mixing of cells. Other types of density-dependent diffusion are considered in modeling GBM migration [19]. Although a more complete picture of cell migration needs to include mechanisms such as chemotaxis and haptotaxis, tumor growth is oftentimes seen as diffusive and a careful choice of diffusion term is believed to be sufficient to model cell migration in many cases. Although the most accurate form of diffusion is debatable in the context of GBM, we note that in our analysis the exact form of diffusion does not matter since the second derivatives are dropped in (2.6). The diffusion coefficient does play an important role in the linearized wave head where it affects the wave speed, and in characteristic length where its square root scales the space. Whereas the scale invariant part of the wave profile is mostly determined by the exact form of birth and death for which we did a thorough exploration. So we believe that our model should capture the essence of the tumor morphology revealed by MR images.

Traveling wave solution is not uncommon in a reaction-diffusion system and studies on this topic date back to [4]. Rigorous proof of existence of traveling wave solution in a reaction-diffusion system often leads to phase space analysis such as in [2]. Not only the high dimension but also the singularity represented in the cross diffusion makes a proof a changeling task, which will the the focus of future work. Nevertheless, the reduced system is reconcilable to phase plane analysis and the orbit representing the traveling wave solution can be identified (see appendix).

Instead of having a lumped proliferation term as in [7] which only tracks net proliferation, our model treats birth and death separately, making it possible to gauge the underlying total proliferation of cancer cells. This is valuable information for personalized treatment design since most chemotherapy and radiotherapy target proliferating cells. Moreover, the structural information is also potential useful, e.g., it may instruct drug dose so that the drug can perfuse through the width of the proliferating rim. Research along this line has been conducted using the PI model [8]. We plan to investigate along this line using our model in the future study.

We recognize the possibility that the tumor is evolving over its course of growth as the observed tumor profile at two different times is not scale invariant. We suspect that the parameters of the model are not constant over time. In this paper, we devise a method which uses two MR images taken at two consecutive times before surgery, and our method is feasible whether the two scans are consistent with invariant tumor profile or not. It is straightforward to extend the current method to make use of MR images taken at three or even more time points. By updating parameters as more data is acquired, we are essentially doing data assimilation. There has been research on applying full-fledged data assimilation to cancer modeling [9, 13]. Our method stands out being simple and computationally light-weighted. In the case when only one per-surgery MR scan is available, we demonstrated a way to estimate parameters involving mild and experimentally verifiable assumptions. The major contributions of this paper

is the novel way to make use of scarce data which are the routinely available in clinical settings. So we hope our method would offer wide and practical use compared to large-scale computational models [3, 16], which often focus on experimental data.

Acknowledgments

The authors would like to thank Leslie Baxter and Leland Ho at Barrow Neurological Institute for providing MR images. The work is supported by Arizona Biomedical Research Commission. NSF NIH.

References

1. Jose Canosa. On a Nonlinear Diffusion Equation Describing Population Growth. *IBM Journal of Research and Development*, 17(4):307–313, jul 1973.
2. StevenR. Dunbar. Travelling wave solutions of diffusive Lotka-Volterra equations. *Journal of Mathematical Biology*, 17(1):11–32, may 1983.
3. S. E. Eikenberry, T. Sankar, M. C. Preul, E. J. Kostelich, C. J. Thalhauser, and Y. Kuang. Virtual glioblastoma: Growth, migration and treatment in a three-dimensional mathematical model. *Cell Proliferation*, 42(4):511–528, 2009.
4. R. A. FISHER. THE WAVE OF ADVANCE OF ADVANTAGEOUS GENES. *Annals of Eugenics*, 7(4):355–369, jun 1937.
5. Philip Gerlee and Sven Nelander. Travelling wave analysis of a mathematical model of glioblastoma growth. *Mathematical Biosciences*, 276:75–81, jun 2016.
6. K. Harley, P. van Heijster, R. Marangell, G. J. Pettet, and M. Wechselberger. Existence of Traveling Wave Solutions for a Model of Tumor Invasion. *SIAM Journal on Applied Dynamical Systems*, 13(1):366–396, jan 2014.
7. Pamela R. Jackson, Joseph Juliano, Andrea Hawkins-Daarud, Russell C. Rockne, and Kristin R. Swanson. Patient-Specific Mathematical Neuro-Oncology: Using a Simple Proliferation and Invasion Tumor Model to Inform Clinical Practice. *Bulletin of Mathematical Biology*, 77(5):846–856, may 2015.
8. Minsun Kim, Jakob Kotas, Jason Rockhill, Mark Phillips, Minsun Kim, Jakob Kotas, Jason Rockhill, and Mark Phillips. A Feasibility Study of Personalized Prescription Schemes for Glioblastoma Patients Using a Proliferation and Invasion Glioma Model. *Cancers*, 9(12):51, may 2017.
9. Eric J Kostelich, Yang Kuang, Joshua M McDaniel, Nina Z Moore, Nikolay L Martirosyan, and Mark C Preul. Accurate state estimation from uncertain data and models: an application of data assimilation to mathematical models of human brain tumors. *Biology Direct*, 6(1):64, dec 2011.
10. Yang Kuang, John D. Nagy, and Stephen E. Eikenberry. *Introduction to mathematical oncology*. Chapman and Hall/CRC.
11. Anotida Madzvamuse, Raquel Barreira, and Alf Gerisch. Cross-Diffusion in Reaction-Diffusion Models: Analysis, Numerics, and Applications. pages 385–392. Springer, Cham, 2017.

12. Nikolay L. Martirosyan, Erica M. Rutter, Wyatt L. Ramey, Eric J. Kostelich, Yang Kuang, and Mark C. Preul. Mathematically modeling the biological properties of gliomas: A review. *Mathematical Biosciences and Engineering*, 12(4):879–905, apr 2015.

13. Joshua McDaniel, Eric Kostelich, Yang Kuang, John Nagy, Mark C. Preul, Nina Z. Moore, and Nikolay L. Matirosyan. Data Assimilation in Brain Tumor Models. pages 233–262. Springer, New York, NY, 2013.

14. Maxwell Lewis Neal, Andrew D. Trister, Tyler Cloke, Rita Sodt, Sunyoung Ahn, Anne L. Baldock, Carly A. Bridge, Albert Lai, Timothy F. Cloughesy, Maciej M. Mrugala, Jason K. Rockhill, Russell C. Rockne, and Kristin R. Swanson. Discriminating Survival Outcomes in Patients with Glioblastoma Using a Simulation-Based, Patient-Specific Response Metric. *PLoS ONE*, 8(1):e51951, jan 2013.

15. Andrew D Norden and Patrick Y Wen. Glioma therapy in adults. *The neurologist*, 12(6):279–92, nov 2006.

16. Erica M Rutter, Tracy L Stepien, Barrett J Anderies, Jonathan D Plasencia, Eric C Woolf, Adrienne C Scheck, Gregory H Turner, Qingwei Liu, David Frakes, Vikram Kodibagkar, Yang Kuang, Mark C Preul, and Eric J Kostelich. Mathematical Analysis of Glioma Growth in a Murine Model. *Scientific reports*, 7(1):2508, 2017.

17. Jonathan A. Sherratt. Wavefront propagation in a competition equation with a new motility term modelling contact inhibition between cell populations. *Proceedings of the Royal Society of London. Series A: Mathematical, Physical and Engineering Sciences*, 456(2002):2365–2386, oct 2000.

18. Jonathan A. Sherratt and Mark A.J. Chaplain. A new mathematical model for avascular tumour growth. *Journal of Mathematical Biology*, 43(4):291–312, oct 2001.

19. Tracy L Stepien, Erica M Rutter, and Yang Kuang. A data-motivated density-dependent diffusion model of in vitro glioblastoma growth. *Mathematical biosciences and engineering : MBE*, 12(6):1157–72, dec 2015.

20. Tracy L. Stepien, Erica M. Rutter, and Yang Kuang. Traveling Waves of a Go-or-Grow Model of Glioma Growth. *SIAM Journal on Applied Mathematics*, 78(3):1778–1801, jan 2018.

21. K. R. Swanson, R. C. Rockne, J. Claridge, M. A. Chaplain, E. C. Alvord, and A. R. A. Anderson. Quantifying the Role of Angiogenesis in Malignant Progression of Gliomas: In Silico Modeling Integrates Imaging and Histology. *Cancer Research*, 71(24):7366–7375, dec 2011.

22. K R Swanson, R C Rostomily, and E C Alvord. A mathematical modelling tool for predicting survival of individual patients following resection of glioblastoma: a proof of principle. *British Journal of Cancer*, 98(1):113–119, jan 2008.

Supplementary (if necessary)

We perform phase plane (w-p plane) analysis of (2.7) to show the existence of a trajectory that starts from $(1,0)$ and ends at $(w^*,0)$ where $w^* \geq 0$ if (2.2) are satisfied. First we note that $(1,0)$ is an unstable fixed point and the trajectory starting here has slope -1 which is the direction of the unstable manifold.

Moreover

$$\frac{d^2p}{dw^2} = \frac{\delta'(w)g(w) - \delta(w)g'(w)}{\rho g(w)^2} < 0$$

for $w \in (0, 1)$ because of the assumptions we had on g and δ. It follows that the trajacory must remain below the line $p = 1 - w$. Assuming $g(w)$ and $\delta(w)$ are continuous, there must be a $w^\dagger \in (0, 1)$ such that $\rho g(w^\dagger) = \delta(w^\dagger)$. For $w > w^\dagger$, the trajectory has positive slope and hence heading down to the w-axis. Since $\frac{dw}{dz}|_{w=0} = 0$, the trajectory cannot cross p-axis. Thus it must intersect the w-axis at some $w^* \in (0, w^\dagger)$

AIMS Press